IEEE Access
Multidisciplinary | Rapid Review | Open Access Journal

Received February 12, 2020, accepted March 10, 2020, date of publication April 2, 2020, date of current version April 27, 2020.

Digital Object Identifier 10.1109/ACCESS.2020.2985107

Self-Guided Limited-Angle Computed Tomography Reconstruction Based on Anisotropic Relative Total Variation

CHANGCHENG GONG[1] AND LI ZENG[2,3,4], (Senior Member, IEEE)

[1]College of Mathematics and Statistics, Chongqing Technology and Business University, Chongqing 400067, China
[2]Chongqing Key Laboratory of Analytic Mathematics and Applications, Chongqing University, Chongqing 401331, China
[3]College of Mathematics and Statistics, Chongqing University, Chongqing 401331, China
[4]Engineering Research Center of Industrial Computed Tomography Nondestructive Testing of the Education Ministry of China, Chongqing University, Chongqing 400044, China

Corresponding author: Li Zeng (drlizeng@cqu.edu.cn)

This work was supported in part by the National Natural Science Foundation of China under Grant 61771003 and Grant 61701174.

ABSTRACT In some computed tomography (CT) applications, limited-angle projections are used for image reconstruction, and traditional reconstruction methods, such as filtered back-projection (FBP) or simultaneous algebraic reconstruction technique (SART), cannot reconstruct high-quality CT images without prior knowledge assistance. For limited-angle CT reconstruction, total variation minimization (TVM) method is not conductive to recovering image structures. Image reconstruction methods based on anisotropic total variation (ATV) and reweighted anisotropic total variation (RwATV) can significantly reduce the shading artifacts using prior knowledge of the scanning angular range and image sparsity. However, using the knowledge of image sparsity does not further improve image quality in some applications. In this paper, we propose a new reconstruction method based on anisotropic relative total variation (ARTV) for limited-angle CT reconstruction. In ARTV, the windowed inherent variation (WIV) indicates the strength of structure information and WIV values are adaptively determined by local structure information. In limited-angle CT, particular scanning angular range urges us into exerting different strengths on different directions of ARTV. Experiments on FORBILD HEAD phantom, a thoracic image and real projections of a walnut are performed to test the new method. Experimental results show that the destroyed structures are recovered to some extent, and we acquire higher image quality compared to some existing limited-angle CT reconstruction methods.

INDEX TERMS Computed tomography, image reconstruction, limited-angle computed tomography, anisotropic total variation, relative total variation.

I. INTRODUCTION

Computed tomography (CT) is used in various applications, such as medical examination [1]–[3], industrial nondestructive testing [4], and security inspection [5], [6]. In medical CT, people pay more and more attention to X-ray radiation dose, since it is harmful to patients [7]. Reducing radiation dose is of realistic significance to patients. To this end, one can reduce the X-ray tube current or the number of projection views. For example, limited-angle CT scanning is a simple and effective way to achieve this goal. Limited-angle CT scanning may be encountered in other applications where projection views are restricted to a limited angular range as shown in Fig. 1. For example, in nondestructive testing of pipeline in service [8], scanning environment forces us to perform CT scanning in a limited angular range; besides, limited-angle CT scanning is used to increase temporal resolution in coronary computed tomography angiography [9]. In micro-CT applications, some detected objects have special structures, such as long objects and discoid objects. At this time, the object can only rotate a limited range due to the limitation of imaging geometry, or the X-ray is completely absorbed in some projection views, resulting in projection loss [10]. In a word, limited-angle CT has

The associate editor coordinating the review of this manuscript and approving it for publication was Yi Zhang.

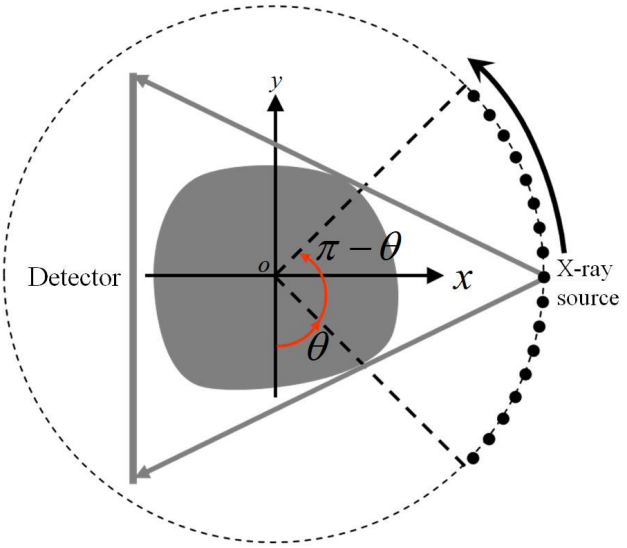

FIGURE 1. Diagram of limited angle CT scan $[\theta, \pi - \theta]$.

attracted more and more attention in recent years. However, for limited-angle CT, FBP cannot reconstruct high-quality CT images, and the reconstructed images often suffer from obvious artifacts. In limited-angle CT, these artifacts resemble shadows and are therefore referred to as the shading artifacts in our work. Iterative reconstruction method SART can reduce partial artifacts, but a more effective approach is to constrain the reconstructed images using appropriate prior knowledge during iterative reconstruction. One of the most commonly used prior assumptions is that CT images are sparse or approximately sparse in the gradient domain. Based on this knowledge, TVM is developed for few-view and limited-angle CT, and it performs better than algebraic reconstruction technique and expectation-maximization algorithm [11]. More specifically, TVM can reconstruct high-quality CT images using few-view projections [11], [12], but the images reconstructed from limited-angle projections still suffer from residual artifacts. TV is defined as the sum of all image gradients, minimizing TV would equally penalize all the image gradients, thus smoothing image structures and weakening structures that are destroyed by the shading artifacts. Some improved methods are proposed for edge-preserving CT reconstruction, such as such as edge-preserving TV [1], adaptive-weighted TV (AwTV) [13] and so on. AwTV method utilizes anisotropy features of image edges to acquire adaptive smoothing. Besides, reconstruction methods based on L_0 norm minimization of wavelet coefficients [14] or image gradient [15] are used to reduce the shading artifacts. L_0 norm directly measure the image sparsity. Minimizing L_0 norm effectively reduces the shading artifacts and does not penalize large image gradients, thus preserving image structures. For some limited-angle CT applications, some prior images are available for image reconstruction, so these images are incorporated into image reconstruction model to further improve image quality [9], [16]. In fact, using prior images can greatly improve reconstructed image quality, but these reconstruction methods often require accurate image registration that is difficult. And unfortunately, in many cases there is no prior image available. For example, in micro-CT applications, a long object may not have a prior image. Besides, the above mentioned reconstruction models using a prior image does not consider the anisotropy characteristics of the limited-angle CT. Based on wavelet frame [14] and guided image filtering (GIF) [17], Wang *et al*. proposed a limited-angle CT reconstruction algorithm [18], where the output result of wavelet frame step is used as the guidance image of GIF step and the output result of SART step is used as the input image of GIF step. In this way, this method does not need prior images. However, this kind of method is not designed according to the characteristics of limited-angle CT reconstruction.

A breakthrough in limited-angle CT reconstruction is the analysis about the reconstructed images and the shading artifacts made by Quinto *et al.* [19]–[21]. Their analysis shows that image edges (including structures and details) that are tangent to transmitted X-rays could easily be reconstructed, otherwise, they would be missing and replaced by the shading artifacts in reconstructed images. In fact, the available projections are distributed in a known limited angular range, which inspires researchers to incorporate this prior knowledge and the above analysis results into reconstruction model to improve image quality. Jin *et al.* proposed an image reconstruction method based on anisotropic total variation (ATV) for limited-angle CT [22]. Then blurred image structures are free from serious regularization constraint, and on the contrary, the data fidelity constraints imposed by the projections make these the structures clear gradually. Following this idea, Chen *et al*. proposed another form of ATV [23]. Due to different recoverability of image structures in different directions, the intensity of the one-dimensional total variation (1D TV) regularization in each direction is variable. The two ATV methods can reduce artifacts in reconstructed images by gently penalizing blurred structures. The idea of ''anisotropy'' is extended to exterior CT [4] and multiple limited-angle CT [24] to reduce the shading artifacts; in these applications, this idea indeed improve image quality. However, ATV is still defined as the weighted sum of image gradients in x and y directions. In order to measure image sparsity more directly, reweighted ATV (RwATV) [25] is used to reduce the dependence of image sparsity measure on image gradients. Using the reweighted technique, RwATV can better approximate image gradient L_0 norm. Therefore, minimizing RwATV subject to constraints imposed by CT projections is conductive to preserving image structures and reducing shading artifacts. Reconstruction method based on ''anisotropy'' and L_0 norm minimization of image gradient is also proposed to reduce shading artifacts [10]. However, L_0 norm minimization is a non-deterministic polynomial-hard problem. All these reconstruction methods show that using the idea of anisotropy has the potential to further improve image quality in limited-angle CT. However, one common

disadvantage of these image gradient based methods is that they cannot effectively distinguish the gradients in image structures and flat regions.

In CT reconstruction, image structures are key information. However, some image structures in limited-angle CT images are missing or weak due to incomplete projections. Therefore, we propose to use "anisotropy" to enhance weak structures. Recently developed relative total variation (RTV) is originally used to extract image structures from regular or irregular background [26]. In addition, RTV and its variant have been applied to different CT reconstruction problems [16], [27]. RTV is defined based on windowed total variation (WTV) and WIV. And WIV can indicate strength of image structures, even if image structures are weak. Therefore, WIV helps preserve structures and suppress artifacts as adaptive weights of WTV. In an image reconstructed from limited-angle projections, some structures are weak due to missing projection views, so isotropic regularization would weaken these structures. In this study, we first define anisotropic WTV (AWTV) and ARTV, and then propose a new reconstruction method based on ARTV measure. We call this method ARTV method for short. In the proposed method, the structures of image itself are represented as adaptive WIV values in the process of image reconstruction. So ARTV method has the ability to extract image structures. Besides, we reasonably adjust constraint strength of regularization on image structures along x and y directions according to the scanning angular range. Experiments on FORBILD HEAD phantom, a thoracic image and real projections of a walnut are performed to test the ARTV method. And we compare it with existing CT reconstruction methods, such as TVM, ATV, AwTV, and RwATV methods. Reconstruction results indicate that ARTV method significantly reduces shading artifacts and performs better than other competing methods.

This paper is organized as follows. In section II, we introduce TVM method and reconstruction methods based on ATV and RwATV, then we define AWTV and ARTV, finally we propose ARTV method. In section III, we test ARTV on FORBILD HEAD phantom and real CT data, and report experimental results. In section IV, we discuss the issues that need further explanation. We give the conclusion of this study in section V.

II. METHODOLOGY

A. CT IMGAING MODEL

In practical CT applications, the projections are approximated by the following linear system,

$$Af = g. \tag{1}$$

where $g = (g_1, g_2, \cdots, g_M)^T$ is the acquired projection data with D detector units at N_p projection views, and $M = N_p \cdot D$. And $f = (f_1, f_2, \cdots, f_P)^T$ is the image vector to be reconstructed. We also use this form of f, $f = \left(f_{i,j}\right) \in \mathbb{R}^{I\times J}$, $i = 1, 2, \cdots, I$ and $j = 1, 2, \cdots, J$; the conversion between this two forms are written as $p = (j-1)\times I + i$. $A \in \mathbb{R}^{M\times P}$ is the system matrix. In limited-angle CT applications, $M < P$, that is to say, image reconstruction is an ill-posed inverse problem.

B. RELATED RECONSTRUCTION MODEL

1) TOTAL VARIATION MINIMIZATION

TVM has been used to suppress artifacts in limited-angle CT. The TV of one image is defined as the sum of image gradients [11],

$$\mathrm{TV}(f) = ||\nabla f||_1 = \sum_{p=1}^{P} \sqrt{\left(\partial_x f_p\right)^2 + \left(\partial_y f_p\right)^2}. \tag{2}$$

where $||\cdot||_1$ denotes the L_1 norm. Thus TV is a L_1 norm, which counts image gradient magnitude. In practice, $\partial_x f_p$ and $\partial_y f_p$ are approximated by difference operators, for example, $\partial_x f_{i,j} \approx f_{i,j} - f_{i-1,j}$, $\partial_y f_{i,j} \approx f_{i,j} - f_{i,j-1}$. Based on this definition, TVM method is written as the optimization problem,

$$\min_f \mathrm{TV}(f) \quad s.t.\ Af = g,\ f \geq 0 \tag{3}$$

TV is a rotationally invariant term, so TVM is direction-irrelevant. Minimizing $\mathrm{TV}(f)$ would equally penalize all image gradients in different directions, and then weak structures in limited-angle CT may be further weakened by TVM.

2) ANISOTROPIC TOTAL VARIATION MINIMIZATION

The scanning angular range is known in limited-angle CT. Jin *et al.* first incorporated this knowledge into reconstruction model and proposed anisotropic total variation (ATV) [22], whose definition is as follows,

$$\mathrm{ATV}(f) = ||\nabla_{\alpha,\beta} f||_1 = \sum_{p=1}^{P} \sqrt{\alpha\left(\partial_x f_p\right)^2 + \beta\left(\partial_y f_p\right)^2}. \tag{4}$$

where α and β are parameters for adjusting weights in x and y directions. Then ATV method is to minimize the measure of ATV subject to constraints imposed by projections. When α and β are the same, ATV degenerates to TV. However, unlike TVM method, ATV minimization is direction-relevant. For example, when $\alpha < \beta$, the difference in x direction contributes less to ATV, then ATV minimization imposes gentle constrains on image gradients in x direction; on the contrary, the data fidelity constraints imposed by the projections make these weak gradients strong gradually.

3) REWEIGHTED ANISOTROPIC TOTAL VARIATION MINIMIZATION

In order to make better use of the prior knowledge of sparsity, reweighted anisotropic total variation (RwATV) combines reweighted technique and ATV measure, and RwATV measure is defined as follows [25],

$$\mathrm{RwATV}(f) = ||\Phi \cdot \nabla_{\alpha,\beta} f||_1 = \sum_{p=1}^{P} \phi_p |\nabla_{\alpha,\beta} f_p|. \tag{5}$$

where $|\nabla_{\alpha,\beta} f_p| = \sqrt{\alpha\left(\partial_x f_p\right)^2 + \beta\left(\partial_y f_p\right)^2}$, and ϕ_p is the element of weight matrix Φ, which is updated iteratively

and defined as $\phi_p^{(k+1)} = \frac{1}{|\nabla_{\alpha,\beta} f_p^{(k)}|+\xi}$, k is the iteration number. The parameter ξ is a small constant to avoid zero denominators. Then RwATV method is to minimize RwATV measure subject to constraints imposed by projections. When all the elements of weight matrix Φ are set to 1, RwATV degenerates to ATV. RwATV method inherits the properties of ATV method, and in addition, the reweighted technique makes the sparsity measure less dependent on image gradients. Therefore, RwATV has greater potential to reconstruct CT images with clear structures and few artifacts.

4) ADAPTIVE-WEIGHTED TOTAL VARIATION MINIMIZATION

The reconstruction method based on AwTV utilizes anisotropy features of image edges to acquire adaptive smoothing. AwTV measure is defined as follows [13],

$$\text{AwTV}(f) = \sum_{i,j} \sqrt{\varpi_{i,j,i-1,j}\partial_x f_{i,j} + \varpi_{i,j,i,j-1}\partial_y f_{i,j}}.$$

where weight $\varpi_{i,j,i-1,j} = \exp\left[-\left(\partial_x f_{i,j}/\delta\right)^2\right]$, and weight $\varpi_{i,j,i,j-1} = \exp\left[-\left(\partial_y f_{i,j}/\delta\right)^2\right]$. Parameter δ is a constant to adjust diffusion strength. Then AwTV method is to minimize AwTV measure subject to constraints imposed by X-ray projections. When parameter δ approaches infinity, the two weights are close to 1, and then AwTV degenerates to TV.

C. ANISOTROPIC RELATIVE TOTAL VARIATION

In this section, we introduce the proposed ARTV reconstruction method. The ARTV measure is defined based on RTV that is originally used for structure extraction.

1) RELATIVE TOTAL VARIATION

The RTV of an image pixel is defined as follows [26],

$$\text{RTV}\left(f_p\right) = \frac{\mathcal{D}_x(p)}{\mathcal{L}_x(p)+\varepsilon} + \frac{\mathcal{D}_y(p)}{\mathcal{L}_y(p)+\varepsilon}. \tag{6}$$

where $\mathcal{D}_x(p)$ and $\mathcal{D}_y(p)$ are called the WTV and defined as follows,

$$\begin{aligned}\mathcal{D}_x(p) &= \sum\nolimits_{q\in\mathcal{W}(p)} h_{p,q}\cdot\left|\left(\partial_x f\right)_q\right|,\\ \mathcal{D}_y(p) &= \sum\nolimits_{q\in\mathcal{W}(p)} h_{p,q}\cdot\left|\left(\partial_y f\right)_q\right|;\end{aligned} \tag{7}$$

where $\mathcal{W}(p)$ is a local rectangular window that is centered as p^{th} pixel of f; $h_{p,q}$ is a Gaussian function whose standard deviation is σ; p and q are image indexes. The definition of WTV indicates that image gradients of image structures and textures or noise increase WTV. $\mathcal{L}_x(p)$ and $\mathcal{L}_y(p)$ are called the WIV and defined as follows,

$$\begin{aligned}\mathcal{L}_x(p) &= \left|\sum\nolimits_{q\in\mathcal{W}(p)} h_{p,q}\cdot\left(\partial_x f\right)_q\right|,\\ \mathcal{L}_y(p) &= \left|\sum\nolimits_{q\in\mathcal{W}(p)} h_{p,q}\cdot\left(\partial_y f\right)_q\right|;\end{aligned} \tag{8}$$

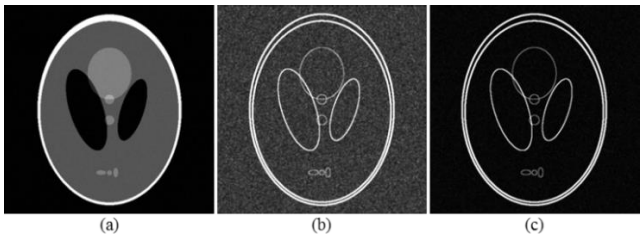

FIGURE 2. (a) A noisy CT image of Shepp-Logan phantom, (b) WTV, (c) WIV.

By this definition, we know that if the signs of $\left(\partial_x f\right)_q$ or $\left(\partial_y f\right)_q$ are the same in $\mathcal{W}(p)$, WIV and WTV values are equal. Otherwise, summing these partial derivative values with different signs may produce a smaller WIV compared to WTV. In fact, most partial derivatives corresponding to edges or structures often have the same sign, while the signs of the partial derivatives generated by noise are mostly random. Therefore, WIV in a noisy region is much smaller than that in a region with more structures. As shown in Fig. 2, image (a) is a noisy image, the WTV image (image (b)) contains the structure information of image (a), but the flat region is polluted by noise. The WIV image (image (c)) indicates the structure information of image (a) and gets rid of most of noise effects. Images in Fig. 2 show that WIV and WTV images are similar in regions with more structures, but WIV value is smaller than WTV value in flat regions. Therefore, WIV values are considered to be well-defined weights of WTV to highlight image structures.

2) ANISOTROPIC WINDOWED TOTAL VARIATION

In this section, we define the anisotropic windowed total variation (AWTV) as follows,

$$\text{AWTV}\left(f_p\right) = \alpha\mathcal{D}_x(p) + \beta\mathcal{D}_y(p), \tag{9}$$

where α and β are weighted parameters. In order to better observe their effects, we display AWTV images in Fig. 3 under several different settings. When α and β are equal, AWTV degrades to WTV, and the AWTV image (Fig. 3(a)) contains complete image gradient information. When α is set to 0.1 (Fig. 3(b)) and 0.01 (Fig. 3(c)), gradient information in x direction contribute less to AWTV image. The definition of AWTV indicates that complete gradient information of an image is composed of that in x direction and y direction. In the reconstructed images in this study, the shading artifacts are distributed in a specific direction that is determined by the scanning angular range. In Fig. 1, the scanning angular range is symmetrical about x-axis, then in the reconstructed images the structures in x direction are weak, while the structures in y direction are strong; in this case, image gradient information in x direction ought to contribute less to AWTV, which makes it easy to preserve image structures and suppress shading artifacts during CT reconstruction. In a word, AWTV has the ability to characterize the gradient information of an image with shading artifacts.

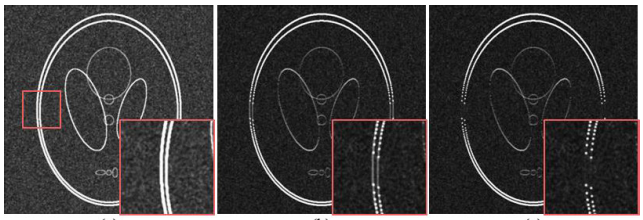

FIGURE 3. AWTV images of Fig. 2(a) with different α and β. (a) $\alpha = 1$ and $\beta = 1$; (b) $\alpha = 0.1$ and $\beta = 1$; (c) $\alpha = 0.01$ and $\beta = 1$; the display window is [0, 0.1]. The close-ups indicate that when α decreases image structures along x direction contribute less to AWTV, and then the image structures would be penalized gently during CT reconstruction.

3) ANISOTROPIC RELATIVE TOTAL VARIATION

Based on the above analysis on RTV and AWTV, we propose ARTV defined as follows,

$$\mathrm{ARTV}\left(f_p\right) = \frac{\alpha \mathcal{D}_x\left(p\right)}{\mathcal{L}_x\left(p\right)+\varepsilon} + \frac{\beta \mathcal{D}_y\left(p\right)}{\mathcal{L}_y\left(p\right)+\varepsilon}, \tag{10}$$

as shown in Fig. 1, when ARTV is optimized, weak constraints are imposed on image structures in x direction, thus leaving room for image structure recovery. Parameter ε is a small constant to avoid zero denominators. On this basis, we propose a new reconstruction method based on ARTV, and we call it ARTV method for short,

$$\min_{f\geq 0} \|Af - g\|_2^2 + \lambda \cdot \sum\nolimits_p \mathrm{ARTV}\left(f_p\right), \tag{11}$$

where λ is the regularization parameter. The first term, known as data fidelity term, imposes constraints generated by X-ray projections; the second term, known as regularization term, preserves image structures and suppresses the shading artifacts. In limited-angle CT reconstruction, parameters α and β are set to different values, in fact, one of them is fixed to 1. For example, in the case shown in Fig. 1, β is set to 1 and $\alpha < \beta$. This setting makes image structure information in x direction contribute less to AWTV; relatively speaking, the data fidelity term is more restrictive in x direction. Therefore, the fidelity of image gradients in x direction becomes stronger under the constraints of projections, and ARTV model can enhance weak structures in limited-angle CT reconstruction.

A two-step algorithm has been used to solve a CT reconstruction model based on RTV iteratively [27]. We also use this algorithm to solve problem (11). The first step is to use SART [28] to acquire an intermediate image $f^{(k+1/2)}$ to fit the data fidelity term, where k is the iteration number. For convenience, the first step is written as follows,

$$f^{(k+1/2)} = \mathrm{SART}\left(f^{(k)}, g\right). \tag{12}$$

Then, the intermediate image is used as the input image of the second step to minimize ARTV measure,

$$\min_{f\geq 0} \sum_p \left[\left(f_p - f_p^{(k+1/2)}\right)^2 + \eta \cdot \mathrm{ARTV}\left(f_p\right)\right]. \tag{13}$$

where η is the newly-formed regularization parameter of problem (13). The numerical solution of this problem can be solved iteratively. Following the strategy in reference [27], we rewritten x part of the measure of ARTV as follows,

$$\begin{aligned}
&\sum_p \frac{\alpha \mathcal{D}_x\left(p\right)}{\mathcal{L}_x\left(p\right)+\varepsilon} \\
&\quad = \alpha \cdot \sum_p \frac{\sum_{q\in\mathcal{W}(p)} h_{p,q} \cdot \left|\left(\partial_x f\right)_q\right|}{\mathcal{L}_x\left(p\right)+\varepsilon} \\
&\quad = \alpha \cdot \sum_{q\in\mathcal{W}(1)} \frac{h_{1,q}}{\mathcal{L}_x\left(1\right)+\varepsilon} \cdot \left|\left(\partial_x f\right)_q\right| + \cdots \\
&\qquad + \alpha \cdot \sum_{q\in\mathcal{W}(P)} \frac{h_{P,q}}{\mathcal{L}_x\left(P\right)+\varepsilon} \cdot \left|\left(\partial_x f\right)_q\right| \\
&\quad = \alpha \cdot \sum_q \sum_{p\in\mathcal{W}(q)} \frac{h_{p,q}}{\mathcal{L}_x\left(p\right)+\varepsilon} \left|\left(\partial_x f\right)_q\right| \\
&\quad \approx \alpha \cdot \sum_q \sum_{p\in\mathcal{W}(q)} \frac{h_{p,q}}{\mathcal{L}_x\left(p\right)+\varepsilon} \frac{1}{\left|\left(\partial_x f\right)_q\right|+\tau} \left(\partial_x f\right)_q^2 \\
&\quad = \alpha \cdot \sum_q u_{x,q} v_{x,q} \left(\partial_x f\right)_q^2.
\end{aligned} \tag{14}$$

where τ is a small constant to avoid zero denominator, and $u_{x,q}$ and $v_{x,q}$ are written as follows,

$$u_{x,q} = \sum_{p\in\mathcal{W}(q)} \frac{h_{p,q}}{\mathcal{L}_x\left(p\right)+\varepsilon} = \left(\mathcal{H}_\sigma * \frac{1}{\mathcal{H}_\sigma * \left(\partial_x f\right)}\right)_q, \tag{15}$$

$$v_{x,q} = \frac{1}{\left|\left(\partial_x f\right)_q\right|+\tau}, \tag{16}$$

where $\mathcal{H}_\sigma$ is a Gaussian filter whose standard deviation is set to σ, and $*$ is convolution operator. Similarly, we rewritten y part of the measure of ARTV as follows,

$$\begin{aligned}
&\sum_p \frac{\beta \mathcal{D}_y\left(p\right)}{\mathcal{L}_y\left(p\right)+\varepsilon} \\
&\quad = \beta \cdot \sum_p \frac{\sum_{q\in\mathcal{W}(p)} h_{p,q} \cdot \left|\left(\partial_y f\right)_q\right|}{\mathcal{L}_y\left(p\right)+\varepsilon} \\
&\quad = \beta \cdot \sum_{q\in\mathcal{W}(1)} \frac{h_{1,q}}{\mathcal{L}_y\left(1\right)+\varepsilon} \cdot \left|\left(\partial_y f\right)_q\right| + \cdots \\
&\qquad + \beta \cdot \sum_{q\in\mathcal{W}(P)} \frac{h_{P,q}}{\mathcal{L}_y\left(P\right)+\varepsilon} \cdot \left|\left(\partial_y f\right)_q\right| \\
&\quad = \beta \cdot \sum_q \sum_{p\in\mathcal{W}(q)} \frac{h_{p,q}}{\mathcal{L}_y\left(p\right)+\varepsilon} \left|\left(\partial_y f\right)_q\right| \\
&\quad \approx \beta \cdot \sum_q \sum_{p\in\mathcal{W}(q)} \frac{h_{p,q}}{\mathcal{L}_y\left(p\right)+\varepsilon} \frac{1}{\left|\left(\partial_y f\right)_q\right|+\tau} \left(\partial_y f\right)_q^2 \\
&\quad = \beta \cdot \sum_q u_{y,q} v_{y,q} \left(\partial_y f\right)_q^2.
\end{aligned} \tag{17}$$

And $u_{y,q}$ and $v_{y,q}$ have the following definitions,

$$u_{y,q} = \sum_{p\in\mathcal{W}(q)} \frac{h_{p,q}}{\mathcal{L}_y(p)+\varepsilon} = \left(\mathcal{H}_\sigma * \frac{1}{\mathcal{H}_\sigma * (\partial_y f)}\right)_q, \quad (18)$$

$$v_{y,q} = \frac{1}{\left|(\partial_y f)_q\right| + \tau}, \quad (19)$$

Then, on the basis of above decomposition, ARTV is rewritten in terms of multiple products, which enables problem (13) to be reformulated as follows,

$$\min_{\mathcal{Q}_f\geq 0} \left(\mathcal{Q}_f - \mathcal{Q}_{f^{(k+1/2)}}\right)^{\mathrm{T}} \left(\mathcal{Q}_f - \mathcal{Q}_{f^{(k+1/2)}}\right) + \eta\cdot\left(\alpha\cdot\mathcal{Q}_f^{\mathrm{T}}\mathcal{G}_x^{\mathrm{T}}\mathcal{U}_x\mathcal{V}_x\mathcal{G}_x\mathcal{Q}_f + \beta\cdot\mathcal{Q}_f^{\mathrm{T}}\mathcal{G}_y^{\mathrm{T}}\mathcal{U}_y\mathcal{V}_y\mathcal{G}_y\mathcal{Q}_f\right), \quad (20)$$

where $\mathcal{Q}_f$ and $\mathcal{Q}_{f^{(k+1/2)}}$ are vector forms of image f and $f^{(k+1/2)}$, $\mathcal{G}_x$ and $\mathcal{G}_y$ are Toeplitz matrices from discrete gradient operators with forward difference. And $\mathcal{U}_x$, $\mathcal{V}_x$, $\mathcal{U}_y$, and $\mathcal{V}_y$ are diagonal matrices with diagonal elements $u_{x,q}$, $v_{x,q}$, $u_{y,q}$, and $v_{y,q}$, respectively. For the sake of convenience, we denote $\alpha\cdot\mathcal{G}_x^{\mathrm{T}}\mathcal{U}_x\mathcal{V}_x\mathcal{G}_x + \beta\cdot\mathcal{G}_y^{\mathrm{T}}\mathcal{U}_y\mathcal{V}_y\mathcal{G}_y$ by $\mathcal{S}$, then minimization problem (20) is transformed into solving a system of linear equations iteratively,

$$\left(I + \eta\cdot\mathcal{S}^{(t)}\right)\cdot\mathcal{Q}_f^{(t+1)} = \mathcal{Q}_{f^{(k+1/2)}}, \quad (21)$$

where I is an identity matrix, t is the iteration number in the second step, and the total iteration number of the second step is denoted by N_{ARTV}; $\left(I+\eta\cdot\mathcal{S}^{(t)}\right)$ is a symmetric positive definite Laplacian matrix. The output image of the second step is denoted by $f^{(k+1)}$ and then it is used for the next iteration until the algorithm terminates.

D. THE RELATIONSHIP BETWEEN ARTV AND TV, ATV, AND RwATV

We first compare the measure of ARTV (equation (10)) and TV (equation (2)). We reorganize ARTV into the form in equation (14) and (17). Newly-formed $u_{x,q}$, $v_{x,q}$, $u_{y,q}$, and $v_{y,q}$ act as weights in equation (14) and (17); if they are set to 1, and $\alpha=\beta$, ARTV degenerates into $\sum_q (\partial_x f)_q^2 + (\partial_y f)_q^2$, which counts image gradient magnitude like TV. If $u_{x,q}$, $v_{x,q}$, $u_{y,q}$, and $v_{y,q}$ are set to 1, and $\alpha\neq\beta$, ARTV degenerates into $\sum_q \alpha\cdot(\partial_x f)_q^2 + \beta\cdot(\partial_y f)_q^2$, which is mathematically equivalent to ATV.

In the definition of RwATV (equation (5)), ϕ_p serves as the weight of $|\nabla_{\alpha,\beta} f_p|$; ϕ_p is small at image edges or structures, while ϕ_p is large at flat regions. Therefore, RwATV has less dependence on image gradients. Compared to RwATV, ARTV has the same properties. In fact, WIV in a noisy region is smaller than that in a region with more structures. Thereby, the reciprocal of WIV value is small at image structures, while it is large at flat regions. So ARTV has the advantages of RwATV. However, ARTV and RwATV are different in essence. It should be pointed out that weight ϕ_p is calculated using two adjacent pixels, and WIV is calculated using pixels in a local rectangular window. More importantly, RwATV is defined on the basis of image sparsity, and its focus is to reconstruct an CT image that is sparse in the gradient domain; ARTV is defined on the basis of this knowledge that WIV in a noisy flat region is smaller than that in a region with more structures, and its focus is to highlight main structures in CT images. In a word, ARTV has the excellent properties of RwATV, and has stronger ability to preserve image structures and suppress noise. Based on the analysis, we know TVM, ATV, and RwATV methods are developed on the basis of image sparsity, while the starting point of ARTV method is to protect image structures. AwTV method considers the anisotropic edge property among neighboring image pixels, but it does not consider the prior information of the scanning angular range, while ARTV method considers structure features of an image and the anisotropy characteristics of limited-angle CT.

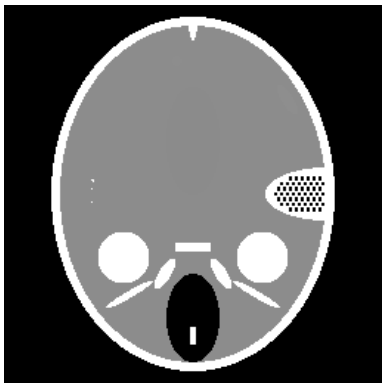

FIGURE 4. CT image of FORBILD HEAD phantom.

III. EXPERIMENTAL RESULTS

Experiments on FORBILD HEAD phantom and real projections of a walnut are performed in this work to test the new method. The used FORBILD HEAD phantom has 256 × 256 pixels; for experiments on this phantom, we assume that the detector is composed of 512 units and the length of the detector is 0.75 × 512 mm. The distance from the X-ray source to the rotation axis is 500 mm, and the distance between the rotation axis and the detector is 250 mm. The phantom itself is used as reference image to calculate root mean square error (RMSE) for image quality comparison, besides, we also calculate peak signal to noise ratio (PSNR), and structural similarity index (SSIM) [29] of reconstructed images. We compare ARTV method to TVM, ATV, AwTV, and RwATV methods.

A. EXPERIMENTS ON FORBILD HEAD PHANTOM

We conduct three group experiments on FORBILD HEAD phantom to compare different reconstruction methods; the phantom is shown in Fig. 4. We add Gaussian noise to the acquired noise-free projections, the mean value is zero, and

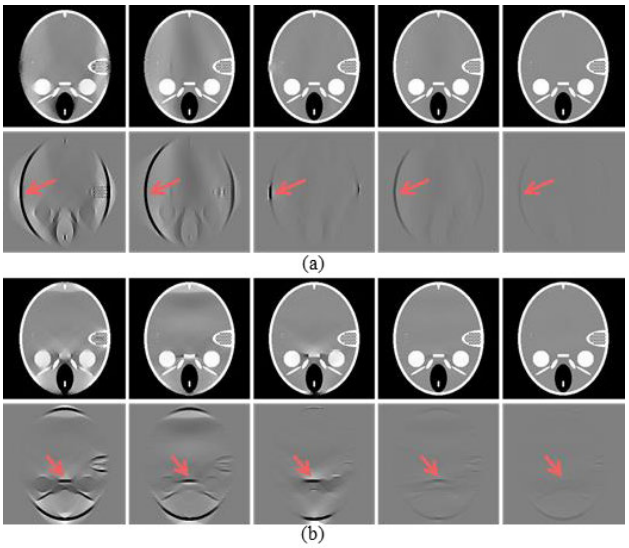

FIGURE 5. Images in experiments on FORBILD HEAD phantom, the projections are in the range of (a) [45°, 135°] and (b) [135°, 225°]. The images from left to right are reconstructed by TVM, ATV, AwTV, RwATV, and ARTV methods in the first row. The images in the second row are difference images between the first-row images and the reference image. The images from left to right are reconstructed by TVM, ATV, AwTV, RwATV, and ARTV methods in the third row, respectively. The images in the fourth row are difference images between the third-row images and the reference image.

the standard deviation is 0.1 percent of the maximum value of the acquired simulation projections. In the first group experiments, the used projections are limited in the range of [45°, 135°] and [135°, 225°]; in the second group experiments, the projections are limited in [30°, 150°] and [120°, 240°]; in the third group experiments, the projections are limited in [15°, 165°] and [105°, 255°], respectively. As shown in Fig. 1, the positive direction of y-axis points to projection view that corresponds to 0°. Different angular ranges are used to evaluate the capability of ARTV in suppressing the shading artifacts. Noisy projections are used for assessing noise suppression capability of these reconstruction methods. Besides, these angular ranges are symmetrical about the axes. For example, [45°, 135°] ([135°, 225°]) is symmetrical about the positive direction of x-axis (y-axis). RMSE, PSNR, and SSIM are used for image quality comparison. Besides, the difference images corresponding to these reconstructed images are used to display the shading artifacts remaining in the reconstructed images. The display windows for reconstructed images and difference images are [0.5, 1.5] and [−0.5, 0.5], respectively.

In the first group experiments, the projections are in the range of [45°, 135°] and [135°, 225°], and the reconstructed images are shown in Fig. 5(a) and Fig. 5(b). The first- and third-row images from left to right are reconstructed by TVM, ATV, AwTV, RwATV, and ARTV methods. We can see that the image reconstructed by TVM suffers from obvious artifacts, and some structures are weak. ATV method can strengthen these weak structures. This result indicates that incorporating angular range into reconstruction model indeed

TABLE 1. The RMSE, PSNR and SSIM of the FORBIHEAD HEAD CT images reconstructed from projections in the range of [45°, 135°] and [135°, 225°].

METHOD	ANGULAR RANGE	RMSE	PSNR	SSIM
TVM	[45°, 135°]	0.1531	21.40	0.8224
ATV		0.0990	25.20	0.8915
AwTV		0.0443	32.17	0.9820
RwATV		0.0213	38.54	0.9883
ARTV		0.0058	49.84	0.9956
TVM	[135°, 225°]	0.1300	22.83	0.8776
ATV		0.0916	25.87	0.9363
AwTV		0.0822	26.81	0.9593
RwATV		0.0141	42.13	0.9907
ARTV		0.0089	46.07	0.9947

TABLE 2. The main reconstruction parameters of TVM, ATV, AwTV, RwATV, and ARTV in the experiments on FORBILD HEAD phantom.

METHOD	ANGULAR RANGE	PARAMETERS
TVM	[45°, 135°]	$\mu = 0.1, N_{TVM} = 20$
ATV		$\mu = 0.2, N_{ATV} = 20, \alpha = 0.01, \beta = 1$
AwTV		$\mu = 0.08, N_{AwTV} = 20, \delta = 0.08$
RwATV		$\mu = 0.2, N_{RwATV} = 20, \alpha = 0.01, \beta = 1, \xi = 0.01$
ARTV		$\eta = 0.0008, \alpha = 0.01, \beta = 1$
TVM	[135°, 225°]	$\mu = 0.1, N_{TVM} = 20$
ATV		$\mu = 0.12, N_{ATV} = 20, \alpha = 1, \beta = 0.02$
AwTV		$\mu = 0.08, N_{AwTV} = 20, \delta = 0.08$
RwATV		$\mu = 0.2, N_{RwATV} = 20, \alpha = 1, \beta = 0.004, \xi = 0.01$
ARTV		$\eta = 0.0008, \alpha = 1, \beta = 0.08$

works for limited-angle CT image reconstruction. However, from the difference images we can see that obvious shading artifacts remain in the images obtained from ATV method. Without using the prior knowledge of the scanning angular range, AwTV method can also reduce the shading artifacts, but some structures of the reconstructed image are lost. RwATV method inherits the advantages of ATV method. And on the basis of ATV method, the measure of RwATV has less dependence on image gradients, which is more convenient to recover weak structures in the iterative process. The images in the fourth column of Fig. 5 show that RwATV method significantly reduces the shading artifacts, and the reconstructed images have clearer structures. This result indicates that the reweighted technique indeed improves image quality by reducing the dependence of sparsity measure on image gradients. From the images in the fourth and fifth column of Fig. 5, we observe that the images obtained by RwATV and ARTV methods have similar quality. However, their corresponding difference images indicate that the images reconstructed by ARTV method are closer to the reference image. In order to evaluate the reconstruction results quantitatively, we calculated their RMSE, PSNR, and SSIM and list them in TABLE 1. From these values, we can obtain the same results. In this group experiments, the main reconstruction parameters of TVM, ATV, AwTV, RwATV, and ARTV are determined by trial and error and are shown in TABLE 2.

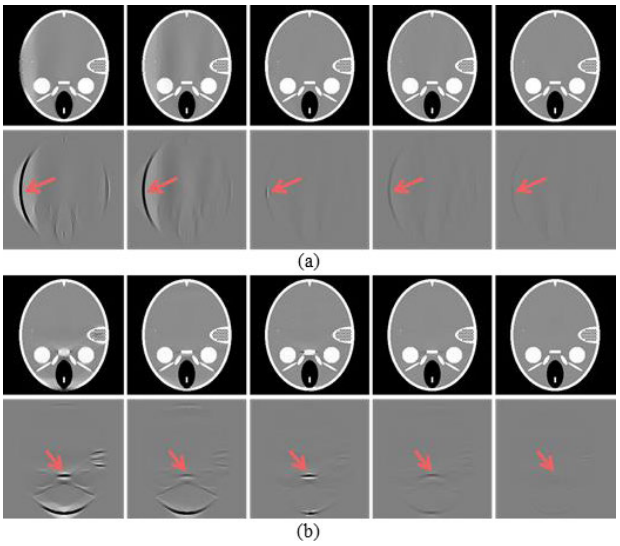

FIGURE 6. Images in experiments on FORBILD HEAD phantom, the projections are in the range of (a) [30°, 150°] and (b) [120°, 240°]. The images from left to right are reconstructed by TVM, ATV, AwTV, RwATV, and ARTV methods in the first row. The images in the second row are difference images between the first-row images and the reference image. The images from left to right are reconstructed by TVM, ATV, AwTV, RwATV, and ARTV methods in the third row, respectively. The images in the fourth row are difference images between the third-row images and the reference image.

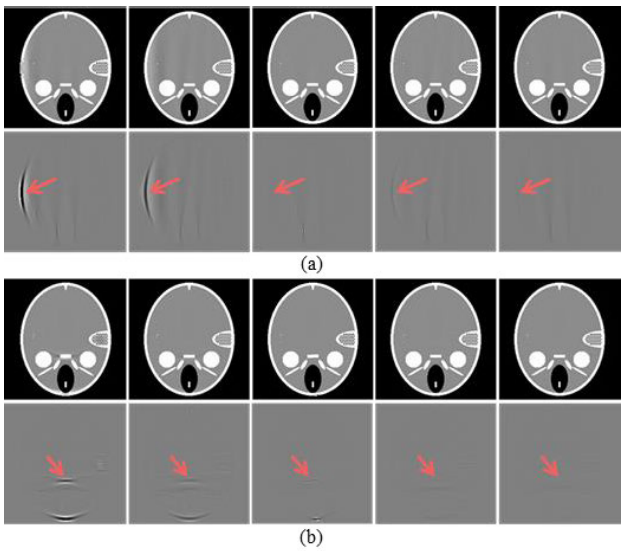

FIGURE 7. Images in experiments on FORBILD HEAD phantom, the projections are in the range of (a) [15°, 165°] and (b) [105°, 255°]. The images from left to right are reconstructed by TVM, ATV, AwTV, RwATV, and ARTV methods in the first row. The images in the second row are difference images between the first-row images and the reference image. The images from left to right are reconstructed by TVM, ATV, AwTV, RwATV, and ARTV methods in the third row, respectively. The images in the fourth row are difference images between the third-row images and the reference image.

Parameter μ represents the step size to reduce image gradient in TVM, ATV, AwTV, and RwATV methods, N_{TVM}, N_{ATV}, N_{AwTV}, and N_{RwATV} represent the number of gradient decent in each step of TVM, ATV, AwTV, and RwATV methods, respectively.

In the second group experiments, the projections are limited in [30°, 150°] and [120°, 240°], and the reconstructed images are shown in Fig. 6(a) and Fig. 6(b). In the third group experiments, the images reconstructed from projections in the range of [15°, 165°] and [105°, 225°] are shown in Fig. 7(a) and Fig. 7(b). As the scanning angular range increases, the reconstructed image quality is gradually getting better. The reconstructed images show that RwATV and ARTV methods perform better than TVM, ATV, and AwTV methods. The difference images indicate that the images reconstructed by ARTV method are closer to the reference image than that reconstructed by AwTV and RwATV methods. In order to evaluate the reconstruction results in Fig.6 and Fig. 7 quantitatively, we calculate their RMSE, PSNR, and SSIM and list them in TABLE 3 and TABLE 4, respectively. From these values, we can obtain the same results. In these two group experiments, the main reconstruction parameters are not listed for the sake of brevity.

For FORBILD HEAD phantom that satisfies the sparsity assumption, ARTV method reconstructs high-quality CT images, which means that ARTV measure also objectively and effectively characterizes image sparsity like RwATV or ATV measure. In fact, the measure of ARTV can be considered as a generalization of ATV. ARTV method inherits the advantages of ATV method, and WIV reduces the dependence of ARTV on image gradients. So ARTV method also has the advantages of RwATV method. Besides, ARTV method has good capability of structure extraction.

TABLE 3. The RMSE, PSNR and SSIM of the FORBIHEAD HEAD CT images reconstructed from projections in the range of [30°, 150°] and [120°, 240°].

METHOD	ANGULAR RANGE	RMSE	PSNR	SSIM
TVM	[30°, 150°]	0.0876	26.56	0.9428
ATV		0.0493	31.25	0.9648
AwTV		0.0122	43.40	0.9706
RwATV		0.0092	45.78	0.9943
ARTV		0.0055	50.24	0.9966
TVM	[120°, 240°]	0.0878	26.24	0.9343
ATV		0.0450	32.04	0.9799
AwTV		0.0389	33.31	0.9598
RwATV		0.0124	43.24	0.9944
ARTV		0.0056	50.15	0.9975

TABLE 4. The RMSE, PSNR and SSIM of the FORBIHEAD HEAD CT images reconstructed from projections in the range of [15°, 165°] and [105°, 255°].

METHOD	ANGULAR RANGE	RMSE	PSNR	SSIM
TVM	[15°, 165°]	0.0502	31.10	0.9818
ATV		0.0257	36.89	0.9878
AwTV		0.0096	45.50	0.9969
RwATV		0.0056	50.12	0.9964
ARTV		0.0051	51.00	0.9974
TVM	[105°, 255°]	0.0461	31.83	0.9730
ATV		0.0162	40.94	0.9950
AwTV		0.0239	37.55	0.9948
RwATV		0.0049	51.37	0.9976
ARTV		0.0047	51.75	0.9982

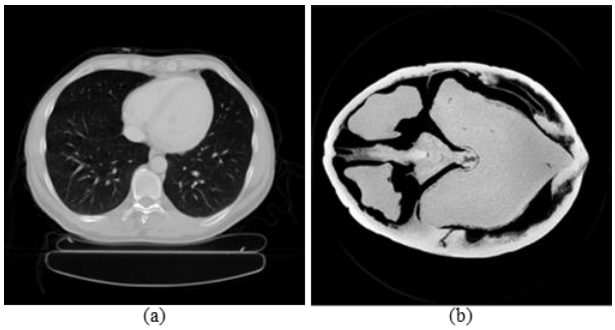

FIGURE 8. Reference images: (a) thoracic image, (b) walnut image and it is reconstructed by SART (10 iterations) using complete-angle projections.

In limited-angle CT, ARTV method recognizes weak structures and recovers them in iterative reconstruction. FORBILD HEAD phantom is sparse in image gradient domain; coincidently, RwATV and ARTV method comply with this fact, thereby, they effectively improve the quality of the reconstruction results. In practice, a normal CT image may not satisfy the sparsity assumption, therefore, it is a promising work to pursue a more effective tool to describe image features. As far as we know, image structures are main features of CT images, so it is promising to improve image quality by focusing on preserving image structures. In order to test ARTV method, experiments on real CT image and CT projections are performed in the next section.

B. EXPERIMENTS ON CT IMAGE FROM TCIA

In this section, one thoracic image obtained from The Cancer Imaging Archive (TCIA) [30] is used to verify the performance of ARTV method, the reference image is shown in Fig.8 (a). The image has 256 $\times$ 256 pixels and it is 200 $\times$ 200 mm^2. The detector is composed of 512 units. The distance from the X-ray source to the rotation axis is 400 mm, and the distance between the rotation axis and the detector is 400 mm. We acquire the simulation projections of the thoracic image following above imaging geometry. Then Poisson noise with incident intensity 1×10^5 is added to the projections; besides, Gaussian noise is also added to the projections, the mean value is zero, and the standard deviation is 0.1 percent of the maximum value of the acquired simulation projections. Projections in the range of [10°, 170°] are used for CT reconstruction in this section. The images reconstructed by TVM, ATV, AwTV, RwATV, and ARTV methods are listed in Fig. 9. We can observe that TVM and ATV reconstruct images with obvious shading artifacts, and some image edges or structures are a little blurry. Their difference images also illustrate this result. AwTV and RwATV methods greatly reduce the shading artifacts. This result shows that using anisotropy features of image edges effectively improve image quality and confirms the validity of the prior information of scanning angular range. However, AwTV and RwATV methods do not further reduce the shading artifacts, while ARTV method greatly reduces these artifacts and the

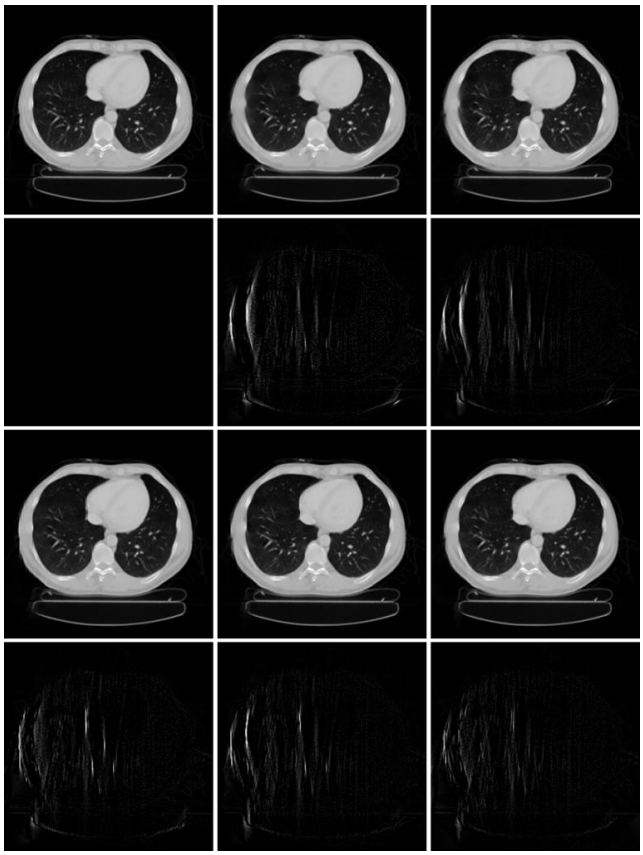

FIGURE 9. Thoracic images reconstructed from projections in the range of [10°, 170°]. In the first-row images, the first one is the reference image, and then the images from left to right are reconstructed by TVM and ATV; the images in the third row are reconstructed by AwTV, RwATV, and ARTV methods, respectively. The images in the second row are difference images between the first-row images and the reference image. The images in the fourth row are difference images between the third-row images and the reference image. The display windows for the reconstructed images and difference images are [0, 0.8] and [0, 0.12], respectively.

reconstructed image has clear structures. The difference images show that the image reconstructed by ARTV method is closest to the reference image. To demonstrate the convergence of the proposed method, the curve of RMSE versus iteration numbers are plotted in Fig. 10 in this experiment, we can see that ARTV method converges to a smaller value quickly.

C. EXPERIMENTS ON REAL CT PROJECTIONS

Experiments on real projections of a walnut are performed to test ARTV method in this section. The complete-angle projections were obtained from Chongqing University and collected by a micro-CT system. We select projections in the center slice of the flat panel detector for two-dimensional CT reconstruction. The image reconstructed by SART algorithm (10 iterations) is used as reference image (Fig. 8(b)) for image quality comparison; the used projections are complete-angle fan-beam projections. In the experiments, the projections of a real walnut for image reconstruction are in the range of [30°, 150°] and [15°, 165°], respectively. The reconstructed

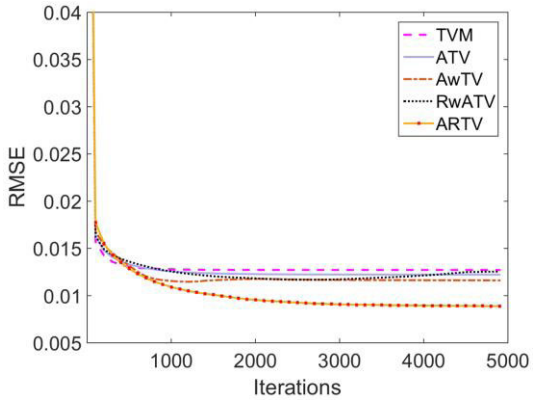

FIGURE 10. The convergence curves of TVM, ATV, AwTV, RwATV, and ARTV methods in experiments on the thoracic image.

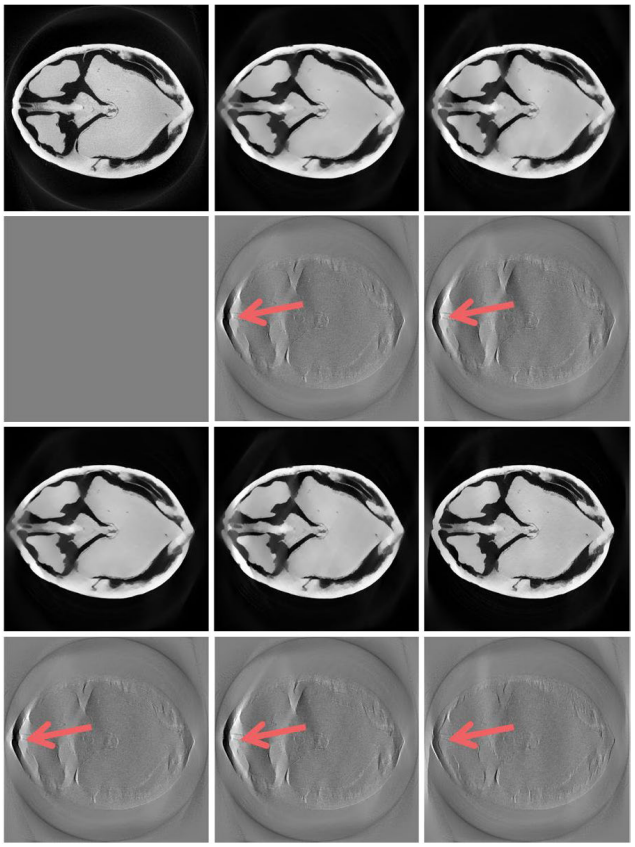

FIGURE 11. CT images of a walnut reconstructed from projections in the range of [30°, 150°]. In the first-row images, the first one is the reference image, and then the images from left to right are reconstructed by TVM and ATV; the images in the third row are reconstructed by AwTV, RwATV, and ARTV methods, respectively. The images in the second row are difference images between the first-row images and the reference image. The images in the fourth row are difference images between the third-row images and the reference image. The display windows for the reconstructed images and difference images are [0, 0.04] and [−0.02, 0.02], respectively.

images are displayed in Fig. 11 and Fig. 12. We observe that TVM reconstructs images with obvious shading artifacts, and image edges or structures are a little blurry. ATV, AwTV, and RwATV methods can reduce the shading artifacts; however,

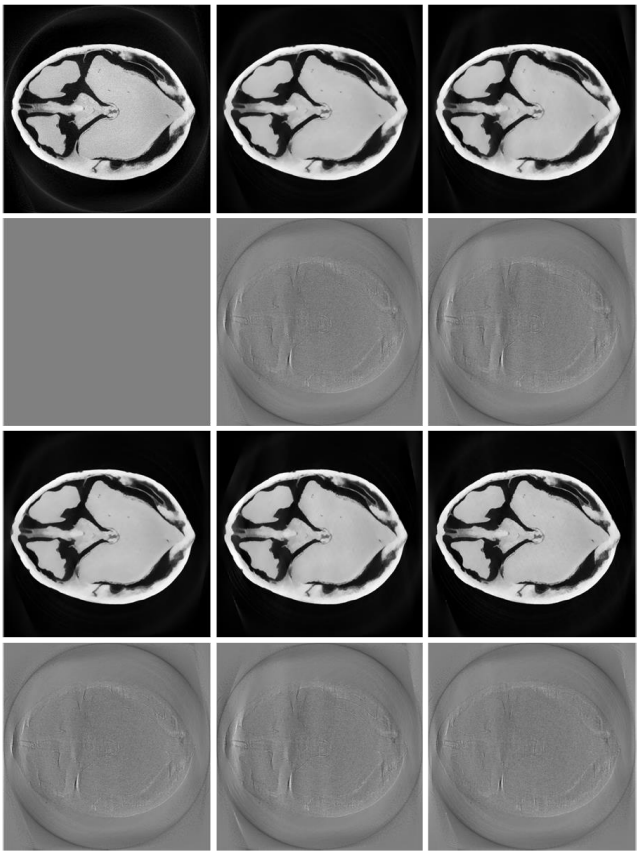

FIGURE 12. CT images of a walnut reconstructed from projections in the range of [15°, 165°]. In the first-row images, the first one is the reference image, and then the images from left to right are reconstructed by TVM and ATV; the images in the third row are reconstructed by AwTV, RwATV, and ARTV method, respectively. The images in the second row are difference images between the first-row images and the reference image. The images in the fourth row are difference images between the third-row images and the reference image. The display windows for the reconstructed images and difference images are [0, 0.04] and [−0.02, 0.02], respectively.

we can still observe residual artifacts. When comparing ATV, AwTV, and RwATV methods, we observe that they reconstruct CT images of similar quality, the difference images also proves this result. This result indicates that using image sparsity cannot further significantly improve image quality in this case. ARTV method further reduces the shading artifacts and the reconstructed image has clear structures. The difference images also show that ARTV method performs best among all competing methods. In this section, the main reconstruction parameters are shown in TABLE 5.

IV. DISCUSSIONS

In this study, ATV and RwATV methods improve image quality using image sparsity and the idea of anisotropy. However, a normal CT image may not be sparse in the gradient domain. We notice that image edges or structures are key information of an image, whether the image is sparse or not. AwTV method considers the anisotropic edge property among neighboring image pixels, but it does not consider the prior information of the scanning angular range. We know RTV can

TABLE 5. The main reconstruction parameters of TVM, ATV, AwTV, RwATV, and ARTV in the experiments on real CT projections.

METHOD	ANGULAR RANGE	PARAMETERS
TVM		$\mu = 0.06, N_{TVM} = 20$
ATV		$\mu = 0.06, N_{ATV} = 20, \alpha = 0.05, \beta = 1$
AwTV	[30°, 150°]	$\mu = 0.06, N_{AwTV} = 20, \delta = 0.05$
RwATV		$\mu = 0.06, N_{RwATV} = 20, \alpha = 0.05, \beta = 1, \xi = 0.001$
ARTV		$\eta = 0.000002, \alpha = 0.3, \beta = 1$
TVM		$\mu = 0.06, N_{TVM} = 20$
ATV		$\mu = 0.06, N_{ATV} = 20, \alpha = 0.1, \beta = 1$
AwTV	[15°, 165°]	$\mu = 0.06, N_{AwTV} = 20, \delta = 0.05$
RwATV		$\mu = 0.06, N_{RwATV} = 20, \alpha = 0.1, \beta = 1, \xi = 0.001$
ARTV		$\eta = 0.000004, \alpha = 0.3, \beta = 1$

effectively highlight the structure information in an image. Inspired by the characteristics of RwATV and RTV, we define AWTV and ARTV measures and then propose ARTV method towards limited-angle CT. In the process of image reconstruction, WIV values guide image reconstruction using the structure information of the current reconstructed image. Experimental results show that ARTV method performs better in preserving image structures and suppressing the shading artifacts than other competing methods. However, there are some related issues that need to be pointed out and further studied in the follow-up works.

A. LIMITATIONS OF ARTV METHOD

The proposed ARTV method focuses on image reconstruction towards limited-angle CT. However, when the available projections are incomplete, some structures of reconstructed images may be missing, not just unclear. At this time, TVM, ATV, AwTV, RwATV, and ARTV methods cannot reconstruct high-quality CT images. Therefore, in ultra-limited-angle CT (for example [0°, 60°]), more information is needed to ensure reconstructed image quality. In this paper, the scanning angular range for experiments on real CT image or projections is at least 120°. In a word, ARTV method is effective, but its ability to suppress artifacts is still limited by incomplete projections.

B. PARAMETERS SELETION

In the ARTV method, we need to determine the values of multiple parameters. But CT image quality is robust to σ, N_{ARTV}, ε, τ, and they are set to 2, 5, 0.001, and 0.001 in this work. Then we need to determine η and α (or β), which significantly affect the reconstructed image quality. For example, in the case shown in Fig. 1, β is set to 1 and $\alpha < 1$. Generally speaking, when the scanning angular range is large, a larger α is conducive to the reconstruction of high-quality CT images. In the extreme case, when the scanning angular range is [0°, 360°], α and β are equal. In actual limited-angle CT reconstruction, a skill may come in handy. We assume that ARTV method gradually recovers image structures, so the image structures with weak strength are also gradually clear; that is to say, image structures are more reliable. At this point, the regularization intensity in x and y directions should get closer, that is, α could be getting larger during CT reconstruction. This skill is optional. In the experiments in this work, η and α (or β) are determined by trial and error. Although the regularization parameter in ARTV method is small compared to other methods, the ARTV term still has a substantial impact on the reconstruction results. We can confirm this conclusion from the experimental results in this paper.

C. SELECTED SCANNING ANGULAR RANGE

In this work, the selected projections are in the angular ranges that are symmetrical about the axes; on the basis of the analysis about the shading artifacts, we know they are also symmetrical about the axes. This setting is to comply with the definition of ARTV measure. In the experiments, the object is placed roughly axisymmetric in coordinates, so the image edges parallel to the axis can be preserved by gentle regularization constraints. In practice, the target object may be placed randomly; and the available projections are distributed in any angular range. We need to point out that the artifact distribution is related to the coordinate system we have established. In practical applications, we can rotate the coordinate system or the reconstructed images to make the artifacts distribute symmetrically about the coordinate axis.

V. CONCLUSION

In this work, we define AWTV and ARTV, and propose the ARTV method for limited-angle CT image reconstruction, and then we clarify the relationship and differences between the measure of ARTV and TV, ATV, and RwATV. Then we describe the solution process of ARTV method. In order to verify the performance of ARTV in suppressing the shading artifacts and preserving image structures, we perform digital phantom experiments and real CT data experiments. In order to comply with the definition of ARTV, the selected scanning angular ranges are symmetrical about the coordinate axes. The graphic comparison and quantitative evaluation indexes in the digital phantom experiments show that ARTV method performs better among all the competing methods. Real CT data experimental results show that the limited-angle CT reconstruction methods based on sparsity constraint has certain limitations, and the ARTV method based on structure extraction can more effectively suppress the shading artifacts and preserve image structures. However, the performance of ARTV method is still limited by incomplete projections. As far as we know, dictionary learning and deep learning are widely used in CT image reconstruction as effective tools. However, they cannot effectively use the prior knowledge widely used in limited-angle CT for image reconstruction, such as the scanning angular range or anisotropy. Nevertheless, we will study limited-angle CT reconstruction methods with stronger ability of suppressing the shading artifacts on the basis of dictionary learning or deep learning in our future research.

REFERENCES

[1] Z. Tian, X. Jia, K. Yuan, T. Pan, and S. B. Jiang, "Low-dose CT reconstruction via edge-preserving total variation regularization," *Phys. Med. Biol.*, vol. 56, no. 18, pp. 5949–5967, Sep. 2011.
[2] H. Han, H. Gao, and L. Xing, "Low-dose 4D cone-beam CT via joint spatiotemporal regularization of tensor framelet and nonlocal total variation," *Phys. Med. Biol.*, vol. 62, no. 16, pp. 6408–6427, 2017.
[3] Y. Gao, Z. Liang, W. Moore, H. Zhang, M. J. Pomeroy, J. A. Ferretti, T. V. Bilfinger, J. Ma, and H. Lu, "A feasibility study of extracting tissue textures from a previous full-dose CT database as prior knowledge for Bayesian reconstruction of current low-dose CT images," *IEEE Trans. Med. Imag.*, vol. 38, no. 8, pp. 1981–1992, Aug. 2019.
[4] Y. Guo, L. Zeng, C. Wang, and L. Zhang, "Image reconstruction model for the exterior problem of computed tomography based on weighted directional total variation," *Appl. Math. Model.*, vol. 52, pp. 358–377, Dec. 2017.
[5] Y. Liu, J. Cheng, Z. Chen, and Y. Xing, "Feasibility study: Low-cost dual energy CT for security inspection," in *Proc. IEEE Nucl. Sci. Symp. Conf. Rec. (NSS/MIC)*, Oct. 2009, pp. 879–882.
[6] B. Gonzales, D. Spronk, Y. Cheng, A. W. Tucker, M. Beckman, O. Zhou, and J. Lu, "Rectangular fixed-gantry CT prototype: Combining CNT X-ray sources and accelerated compressed sensing-based reconstruction," *IEEE Access*, vol. 2, pp. 971–981, 2014.
[7] A. B. de González and S. Darby, "Risk of cancer from diagnostic X-rays: Estimates for the UK and 14 other countries," *Lancet*, vol. 363, no. 9406, pp. 345–351, Jan. 2004.
[8] W. Yu and L. Zeng, "Iterative image reconstruction for limited-angle inverse helical cone-beam computed tomography," *Scanning*, vol. 38, no. 1, pp. 4–13, Jan. 2016.
[9] G.-H. Chen, J. Tang, and J. Hsieh, "Temporal resolution improvement using PICCS in MDCT cardiac imaging," *Med. Phys.*, vol. 36, pp. 2130–2135, May 2009.
[10] J. Xu, Y. Zhao, H. Li, and P. Zhang, "An image reconstruction model regularized by edge-preserving diffusion and smoothing for limited-angle computed tomography," *Inverse Problems*, vol. 35, no. 8, Aug. 2019, Art. no. 085004.
[11] E. Y. Sidky, C.-M. Kao, and X. Pan, "Accurate image reconstruction from few-views and limited-angle data in divergent-beam CT," *J. X-Ray Sci. Technol.*, vol. 14, no. 2, pp. 119–139, 2006.
[12] E. Y. Sidky and X. Pan, "Image reconstruction in circular cone-beam computed tomography by constrained, total-variation minimization," *Phys. Med. Biol.*, vol. 53, no. 17, pp. 4777–4807, Sep. 2008.
[13] Y. Liu, J. Ma, Y. Fan, and Z. Liang, "Adaptive-weighted total variation minimization for sparse data toward low-dose X-ray computed tomography image reconstruction," *Phys. Med. Biol.*, vol. 57, no. 23, pp. 7923–7956, Dec. 2012.
[14] L. Zeng and C. Wang, "Error bounds and stability in the L_0 regularized for CT reconstruction from small projections," *Inverse Problems Imag.*, vol. 10, no. 3, pp. 829–853, Aug. 2016.
[15] W. Yu, C. Wang, and M. Huang, "Edge-preserving reconstruction from sparse projections of limited-angle computed tomography using ℓ_0-regularized gradient prior," *Rev. Sci. Instrum.*, vol. 88, no. 4, Apr. 2017, Art. no. 043703.
[16] C. Gong, L. Zeng, and C. Wang, "Image reconstruction model for limited-angle CT based on prior image induced relative total variation," *Appl. Math. Model.*, vol. 74, pp. 586–605, Oct. 2019.
[17] K. He, J. Sun, and X. Tang, "Guided image filtering," *IEEE Trans. Pattern Anal. Mach. Intell.*, vol. 35, no. 6, pp. 1397–1409, Jun. 2013.
[18] J. Wang, C. Wang, Y. Guo, W. Yu, and L. Zeng, "Guided image filtering based limited-angle CT reconstruction algorithm using wavelet frame," *IEEE Access*, vol. 7, pp. 99954–99963, 2019.
[19] E. T. Quinto, "Tomographic reconstructions from incomplete data-numerical inversion of the exterior radon transform," *Inverse Problems*, vol. 4, no. 3, pp. 867–876, Aug. 1988.
[20] J. Frikel and E. T. Quinto, "Characterization and reduction of artifacts in limited angle tomography," *Inverse Problems*, vol. 29, no. 12, Dec. 2013, Art. no. 125007.
[21] E. T. Quinto, "Artifacts and visible singularities in limited data X-ray tomography," *Sens. Imag.*, vol. 18, no. 1, p. 9, Dec. 2017.
[22] X. Jin, L. Li, Z. Chen, L. Zhang, and Y. Xing, "Anisotropic total variation for limited-angle CT reconstruction," in *Proc. IEEE Nucl. Sci. Symp. Med. Imag. Conf.*, Oct. 2010, pp. 2232–2238.
[23] Z. Chen, X. Jin, L. Li, and G. Wang, "A limited-angle CT reconstruction method based on anisotropic TV minimization," *Phys. Med. Biol.*, vol. 58, no. 7, pp. 2119–2141, Apr. 2013.
[24] C. Gong, L. Zeng, Y. Guo, C. Wang, and S. Wang, "Multiple limited-angles computed tomography reconstruction based on multi-direction total variation minimization," *Rev. Sci. Instrum.*, vol. 89, no. 12, Dec. 2018, Art. no. 125121.
[25] T. Wang, K. Nakamoto, H. Zhang, and H. Liu, "Reweighted anisotropic total variation minimization for limited-angle CT reconstruction," *IEEE Trans. Nucl. Sci.*, vol. 64, no. 10, pp. 2742–2760, Oct. 2017.
[26] L. Xu, Q. Yan, Y. Xia, and J. Jia, "Structure extraction from texture via relative total variation," *ACM Trans. Graph.*, vol. 31, no. 6, pp. 1–10, Nov. 2012.
[27] C. Gong and L. Zeng, "Adaptive iterative reconstruction based on relative total variation for low-intensity computed tomography," *Signal Process.*, vol. 165, pp. 149–162, Dec. 2019.
[28] A. Andersen, "Simultaneous algebraic reconstruction technique (SART): A superior implementation of the ART algorithm," *Ultrason. Imag.*, vol. 6, no. 1, pp. 81–94, Jan. 1984.
[29] Z. Wang, A. C. Bovik, H. R. Sheikh, and E. P. Simoncelli, "Image quality assessment: From error visibility to structural similarity," *IEEE Trans. Image Process.*, vol. 13, no. 4, pp. 600–612, Apr. 2004.
[30] K. Clark, B. Vendt, K. Smith, J. Freymann, J. Kirby, P. Koppel, S. Moore, S. Phillips, D. Maffitt, M. Pringle, L. Tarbox, and F. Prior, "The cancer imaging archive (TCIA): Maintaining and operating a public information repository," *J. Digit. Imag.*, vol. 26, no. 6, pp. 1045–1057, Dec. 2013.

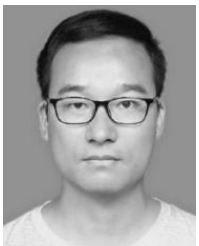

CHANGCHENG GONG received the B.S. degree in information and computing science and the Ph.D. degree in instruments science and technology from Chongqing University, Chongqing, China, in 2014 and 2019, respectively.

From 2014 to 2019, he did doctoral research with the Engineering Research Center of Industrial Computed Tomography Nondestructive Testing of the Education Ministry of China, Chongqing University. He is currently with the College of Mathematics and Statistics, Chongqing Technology and Business University, Chongqing. His main research interests include digital image processing and CT image reconstruction.

LI ZENG (Senior Member, IEEE) received the B.S. degree from Sichuan Normal University, in 1986, the M.S. degree from the Dalian University of Technology, in 1989, and the Ph.D. degree from Chongqing University, in 1997. He held a post-doctoral position with the University of Basel, Switzerland, from 2000 to 2001. He is currently a Professor and a Ph.D. Supervisor with Chongqing University. His research interests include CT image reconstruction, image segmentation, and artificial intelligence algorithm and its application.